Egyptian Journal of Chemistry

http://ejchem.journals.ekb.eg/

Zinc titanate/silica nanopowders formed via sol gel reaction and their physical properties

Ali B. Abou Hammad[1], A. M. Mansour[1], Ahmed M. Bakr[2*], Amany M. El Nahrawy[1*]

[1]*Solid State Physics Department, Physics research Institute, National Research Centre, 33 El Bohouth St., Dokki, Giza 12622, Egypt.*

[2]*Spectroscopy Department, Physics research Institute, National Research Centre, 33 El Bohouth St., Dokki, P.O. 12622, Giza, Egypt*

Abstract

Zinc titanate/silica precursor nanopowders were formed from the raw materials of zinc nitrate, titanium isopropoxide and tetraethyorthosilicate using sol gel route at acidic environment. The phase formation, thermal, and terahertz mechanism of the prepared nanopowders was investigated using X-ray diffraction and Full Prof software), scanning electron microscopy, Thermogravimetric analysis, and Terahertz Time-Domain Spectroscopy System. The XRD analysis of nanopowders combined with Rietveld construction refinement allowed determination of crystalline phases to present and their structural parameters. SEM morphology of the nanopowders is nearly fine spherical with a narrow distribution centered at about 20 nm. Increased introduction of silica decreases the calcination temperature and decreases the terahertz absorption coefficient.

Keywords: $ZnTiO_3$; Terahertz properties; thermal properties; X-ray diffraction; Oxides.

1. Introduction

Because of its ability in many technologies such as electronics, sensing, catalysis, and photonics, the fabrication of nanocomposites has piqued the curiosity of various researchers [1][2][3]. The semiconductor nanocomposites, for example, have been widely employed in the production of optoelectronic devices that function in the blue and ultraviolet (UV) bands [4][5]. The ability of zinc oxide (ZnO) to create a variety of composites has been established. ZnO is an n-type (II-VI group) semiconductor [6]. Metal oxides nanocomposites have attracted significant interest in research because of their technical and industrial importance due to their catalytic, magnetic, optical, and electrical properties along with their enhanced physical and chemical stability [7][8]. Metal oxides are the most assorted band of compounds with unique characteristic properties due to the great variety of crystalline structures and polymorphism, covering from solid-state physics to materials science [9][10][11][12].

Zinc oxide belongs to II-VI semiconductor material. It is an important oxide in the semiconducting metal oxide class owing to its usage in the field of piezoelectricity and transparent semiconducting industry, optical transmittance, and good electrical conductivity [13]. In metal oxides, hexagonal-shaped phase ZnO owns an important place attributable to its characteristic properties and a broad range of applications [13]. ZnO is reported to have applications in diodes, gas sensors, optoelectronic devices, and dye-sensitized solar cells [14][15]. Titanium dioxide (TiO_2) is a member of the most crucial metal oxides for various kinds of industrial applications related to catalysis like selective reduction of NOx gases, photocatalysis for pollution control, organic synthesis, used as a white

*Corresponding author e-mail: amany_physics_1980@yahoo.com ; (Amany M. El Nahrawy), ahmedbakr_8@yahoo.com; (Ahmed M. Bakr).
Receive Date: 31 December 2021; Revise Date: 30 January 2022; Accept Date: 08 March 2022.
DOI: 10.21608/EJCHEM.2022.114039.5185 .

pigment in paints, photovoltaic devices, sensors, as a food additive, in cosmetics and as a potential tool in cancer treatment [16]. Due to their low exciton Bohr radii, “quantum-confinement” or “quantum-size effect” is limited to very low sizes. It means that there is significant scope for the development of novel chemical or physical applications for nanomaterials with few nanometers size [17, 18].

The phase diagram of the ZnO-TiO_2 system is well known to have a temperature above 1000 °C. At lower temperatures, there is more uncertainty regarding the stability of the zinc titanates; Zn_2TiO_4, $ZnTiO_3$, and $Zn_2Ti_3O_8$. Zinc metatitanate $ZnTiO_3$ has a perovskite structure [19, 20]. Perovskite is a natural mineral with the composition of $CaTiO_3$. From there emerged a general formula for Perovskites ABX_3 and has an idealized cubic structure. The ideal crystal structure of cubic perovskite ABX3 has corner-sharing [BX_6] octahedra [3, 21]. The A cations occupy a 12-fold coordination site formed in the center of the cube of eight [BX6] octahedra. The ideal cubic perovskite structure is not very common and also the mineral perovskite itself is slightly distorted. Reduced symmetry found in distorted perovskites is an important parameter for their application as magnetic and electronic materials. Cubic close-packed lattice (ccp) is formed by the combination of a large oxide ion with a metal ion having a small radius. Metal ion occupies the octahedral interstitial sites similar to that of rock salt structure. Substituting one-fourth of the oxygen with a cation of almost the same radius as oxygen like alkali, alkali earth or rare-earth elements reduces the number of octahedral voids, occupied by a small cation to one fourth [22]. The chemical formula of such materials can be written as ABX_3 and the crystal structure is called perovskite [22]. X is often oxygen but also other large ions such as F- and Cl- are possible. Most of the perovskites do not have the ideal cubic structure. They have distorted cubic structures. Jahn-Teller effect, deviations from ideal stoichiometric composition, and size-related effects are the three main reasons for distortion in perovskites [22].

Materials synthesis plays a significant role in tailoring the physical properties of materials. Synthesis of complex metal oxides with appropriate composition, crystal structure, and properties for desired applications is a major challenge in materials chemistry [23][24][25][26]. The sol-gel method is an adaptable process that is used to synthesis various oxide materials [27]. This synthetic method which is most commonly used allows the regulation of the texture of the particles synthesized, also the morphological properties and the chemical properties of the solid materials [28]. This process [5, 6] is a much better replacement for all other methods which are being used for the synthesis of nanoparticles because it will allow impregnation or co-precipitation, which is used for the introduction of dopants. The most important advantages of the sol-gel method include a mixture of molecular scale, the precursor's high purity, and the products obtained from the sol-gel method are homogeneous with a high purity of physical and other properties [21, 29][30][27]. In a pure sol-gel technique, a suspension of colloidal is formed from the hydrolysis and polymerization by the reactions which take place in the precursors which are inorganic metal salt [31, 32][33]. These can also be metal-organic compounds for example metal alkoxides etc. Any of these factors which can affect any of the reactions generally affect the properties of the gel and are commonly referred to as sol-gel parameters which will include types of precursors, the different types of solvents, the water content i.e., acid or base content, the concentration of the precursor, and the last parameter is temperature [34,35][31]. All these parameters can generally affect the structure of the initial gel. Also at all subsequent processing steps the properties of the material. Aging is known as the time taken in the formation of a gel and turns the time taken by it in drying [36]. A gel continues to undergo hydrolysis and condensation but it is not static during aging [37][38]. Wu et al. and Amany et al. reported that the crystallization of co-doped $ZnTiO_3$ synthesized by a sol-gel method took place over 500°C up to 900°C [39][40]. The dissolution and re-precipitation of particles can occur due to the syneresis process [21]. The syneresis process is known as the expulsion of the solvent because of the shrinkage of the gel and its coarsening. This phenomenon may influence both the structural and chemical properties of the product [31]. In this work, we attempt to form silica/ $ZnTiO_3$ nanopowder at a lower temperature, and the structural, thermal, and terahertz properties of the resulting silica doped $ZnTiO_3$ were examined.

2. Experimental work

Silica/Zinc titanate nanopowders were prepared using the sol-gel reaction. These nanopowders are formed to expend zinc acetate; $(O_2CCH_3)_2Zn$, titanium isopropoxide; Ti $(OCH(CH_3)_2)_4$, and tetraethyorthosilicate, HCl, and acetylacetone ($CH_3COCH_2COCH_3$, AcAc). Dissolving the weighted amounts of both zinc acetate was hydrated in distilled water and acetic acid (CH_3COOH) while the stoichiometric amounts (titanium isopropoxide and silica) were dissolved directly in AcAc [40][41]. Tetraethyl orthosilicate was selected as a SiO_2 precursor due to its better incorporation in the $ZnTiO_3$ matrix oxides precursors. The solution of Zn and Ti was added drop-wise to solution SiO_2 solution under vigorous stirring to form a sol. After mixing the raw materials with their solvents, the solutions were vigorously magnetic, stirring for 2h. The synthetic consistent solutions were dehydrated on the hotplate at 150°C until producing the various xerogel samples and then calcined at 500°C.

Characterization

The composition of the samples was recorded by (Philips X'Pert) X-ray diffractometer using the Cu Ka radiation [42]. The microstructures were examined using scanning electron microscopy (SEM Quanta, FEG 250) [43]. Thermo gravimetric (TG) was carried out with a thermal analyzer (TA, SDT-Q600, U.S.A.) in a N2 flow. All terahertz measurements were carried out using TPS spectra 3000 system (Teraview Ltd. England) model by using the ATR unit (35) with silicon crystal and under Nitrogen gas N2 purging. The measuring range was between 60 GHz and 3 THz (2 cm^{-1} - 100 cm^{-1}) and the number of scans was 1800 scan/sec with spectral resolution of 1.2 cm^{-1} [5].

3. Results and discussion

3.1. Phase structure (XRD)

The formation of single-phase $ZnTiO_3$ is usually difficult because of the decomposition of $ZnTiO_3$ into TiO_2 and Zn_2TiO_4 phases above 900°C [44]. Figure (1) XRD patterns performed on the nanopowder calcined at 500°C shows that the TiO_2 and Zn_2TiO_4 don't present.

The FullProf software was employed to obtain the Rietveld refinement of ZTS using the pseudo-Voigt fitting model [45]. The refinement with a linear interpolation background [46], the symmetry parameters, the symmetry parameters, and halfwidth and unit cell parameters mixing coefficient met to χ^2= 8.66%. The expected structure was then refined by fixing the instrumental and profile parameters. Rietveld refinement of pure ZTS sample (as shown in Fig.1 a) gives a refined as a cubic Zn_2TiO_4 phase with parameters of a=8.46479 Å, b=8.46479 Å, c=8.46479 Å, V=606.5249 Å^3, and α=β=γ=90◦. This result is in good agreement with the works published before such as [47–52]. The plans indices are mentioned on the peaks as obtained from the Rietveld refinement.

By the same way, the SiO_2 doped ZTS Rietveld refinement (as shown in Fig.1 b) gives a refined as a triclinic $ZnTi(Si_2O_5)_2$ phase with parameters of a=7.49180 Å, b=7.55428 Å, c=15.83810 Å, V=882.6673 Å^3, and α=93.3497°, β=95.2441°, γ=97.5252°. The plans indices are mentioned on the peaks as obtained from the Rietveld refinement. The 3d molecular structures of pure and SiO2 doped zinc titanate were generated by VESTA-win64 and represented in Fig. 1 (c and d), respectively.

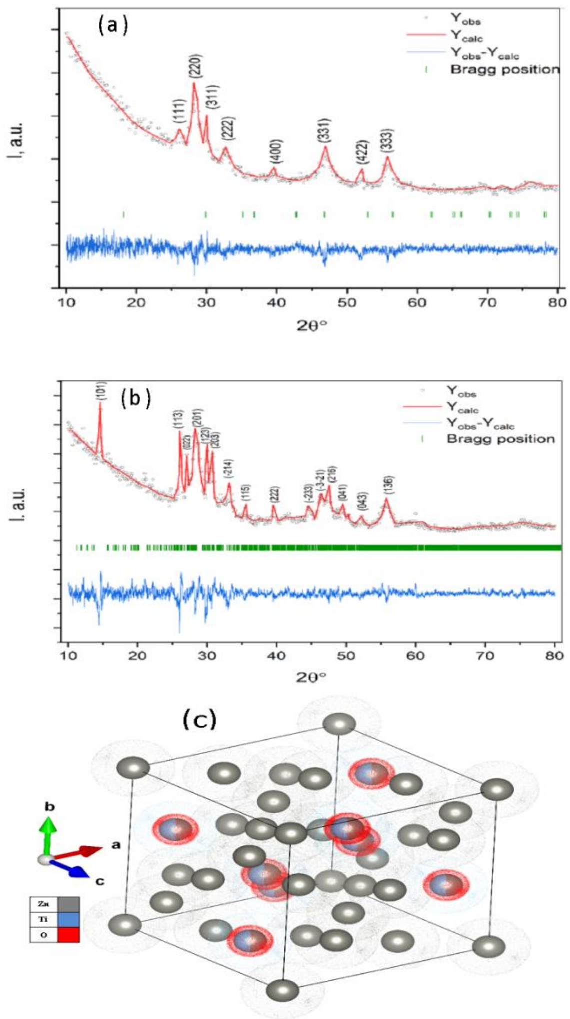

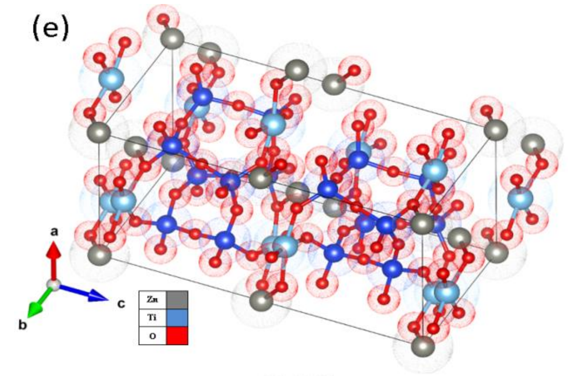

Fig. 1. Rietveld refinement of (a) pure ZTS sample and (b) the SiO_2 doped zinc titanate Rietveld refinement. The 3D representation of (c) Pure and (d) SiO_2 doped zinc titanate.

3.2. SEM

Fig. 2 shows the detailed SEM images of the $ZnTiO_3$ doped SiO_2 materials. In the SEM micrographs, it is obvious that different SiO_2 content does effect too far on the surface morphology and pore size. It can be perceived that the morphology of the nanopowders is nearly fine spherical with a narrow distribution centered at about 20 nm for the spamles formed at 500 °C. The grain shape and size for SiO_2 doped samples are slightly smaller than that of the $ZnTiO_3$ materials. The grains of SiO_2-doped $ZnTiO_3$ are nearly less than 50 nm.

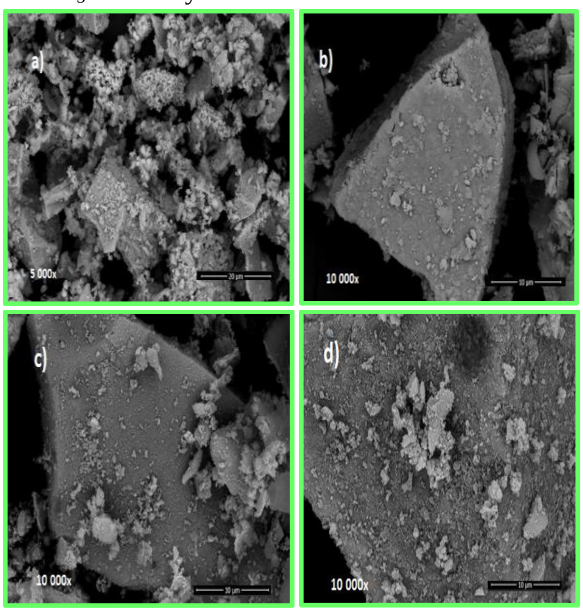

Fig. 2. SEM pictures of $ZnTiO_3$ doped with various SiO_2 particles prepared by sol–gel method at 500°C.

3.3. TGA

Thermal analysis techniques are group of techniques in which a physical property of a substance and its reaction products is measured as a function of temperature where the substance (some analysis need an inert thermal reference) is subjected to a controlled heating process [53]. In the present study, the thermal analyses of the samples are carried out by thermogravimetric analysis (TGA) and differential scanning calorimetric (DSC) analysis, which are usually applied for the evaluation and comparison of the thermal stabilities of different materials [54]. Thermogravimetric analysis (TGA) is an inherently quantitative and extremely powerful thermal technique, in which changes in the mass of a sample are studied while the sample and reference are subjected to a controlled temperature program [53, 54]. Up to 1000°C, TGA can be used to guess the thermal stability of materials and also it may be used to determine the materials composition. Weight gain or loss due to different thermal process, i.e. dehydration, oxidation, or decomposition, can be analyzed by TGA approach [55, 56].

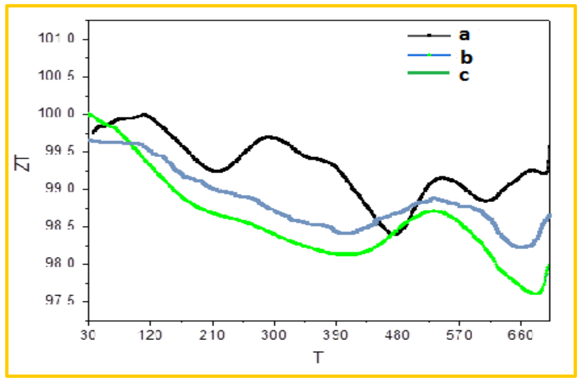

Fig. 3. TGA of $ZnTiO_3$ doped with various (1, 3 mol.%) SiO_2 particles prepared by sol–gel method at 500°C.

In the present study, TA-60WS Thermal Analyzer Shimadzu was used to perform the thermal studies of $ZnTiO_3$-$SmFeO_3$ in the temperature range 30-700°C at a heating rate of 10°C/min in an inert atmosphere using alumina crucibles. The TGA curves of $ZnTiO_3$ sample and doped (1,3 mol.%) SiO_2 are depicted in Fig. 3. Both samples show a small mass change with temperature increase where the total mass loss of both samples did not exceed ≈3% of the initial mass through a heating range of 30-700°C. For the $ZnTiO_3$ sample, the mass loss occurs in five stages: 30-106, 106-220, 274-328, 328-453, and 527-571. The first and second stages occurs between 30 and 220°C corresponding to dehydration process (evaporation of water) [57–60]. The dehydration of $ZnTiO_3$ was reported before by Labus et. Al. [61] and also by Sirajudheen et. Al. [62]. The third small loss stage, between 274 and 328°C, may corresponds to the loss of some organic residual that was existed during the preparation process. The stage occurs between 328 and 453°C corresponding to the crystallization process of zinc titanites [57, 63]. The final stage between 527-571°C is assigned as the melting of the compound [64].

3.4.THz spectroscopy

The spectra of time-dependent electric field $E(t)$ of the THz wave are presented in Fig.4 (a) and were declared with and without the samples by employing attenuated total reflection unit (ATR) with silicon crystal, while the electric field $E0(t)$ via the silicon substrate crystal was employed as a reference. The companion amplitude $|E_s(\omega)|$, $|E_r(\omega)|$ and the phase spectra $\phi_s(\omega)$, $\phi_r(\omega)$ were then acquired by using Fourier transformation as illustrated in Fig.4. (b, c). Clearly, it can be observed directly a notable increase of THz waves reflected from the surface of the sample as the silicon content increase. The phase shift of the transmitted to incident wave $\phi(\omega)$ can be instantly extracted for the measured THz signal since the electric field is registered as a function of time. The THz pulse is delayed in time after propagating through the sample and this is matching to a phase shift of every THz wave included in THz pulse. The absorption coefficient α, and the refractive index n can be obtained by using the following equations:

$$\alpha(\omega) = \frac{1}{d} ln \frac{|Es(\omega)|}{|Er(\omega)|} \quad (1)$$

$$n = 1 + \frac{[\phi s(\omega) - \phi r(\omega)]\,\mathrm{c}}{d\omega} \quad (2)$$

Where the sample thickness $d \approx 200$ μm. The absorption coefficient spectra in the THz frequency range for the samples are given in Fig. 1 (e). obviously, there is a decrease in the absorption coefficient value as the silica content increase in the samples. The terahertz absorption peaks for zinc titanate sample were observed at around 1.1, 1.45, 1.6, 1.9, and 2.2. The terahertz absorption peaks gradually attenuated as the silicon concentration increase in the silicon zinc titanate samples. These THz absorption peaks may be associated to the collective oscillations of the free electrons (plasmons) through the zinc titanate structure. The same behavior was observed in the absorption spectra.

The THz refractive indices (n) for the zinc titanate and silicon zinc titanate samples changes from 1.97–1.94 in 0.2–2.9 THz range and slightly increase in the higher THz as it shown in fig.1. (f).

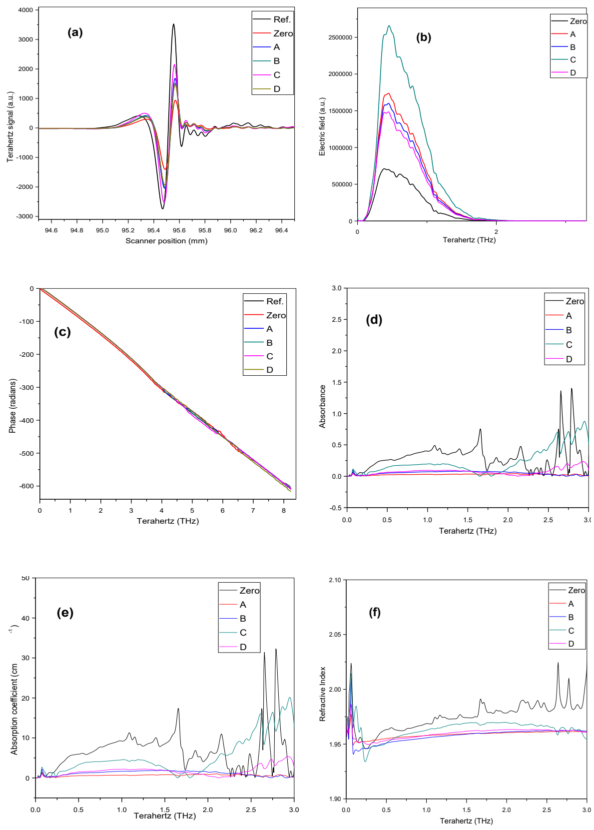

Fig.4. (a) The time-dependent electric field Es(t), Eo(t) for the silicon substrate and for Silica Zinc Titanate samples, (b) The samples spectra: Fourier transforms of the corresponding time-domain signals, (c) Sample Phase, (d) Absorbance, (e) Absorption coefficient, and (f) Refractive Indices for Silica /Zinc Titanate samples.

4. Conclusion

Doped $ZnTiO_3$ with different contents of silica has been formed successfully using sol gel reactions. The formation of triclinic $ZnTi(Si_2O_5)_2$ phase takes place at 500 °C with high phase stability. The effects of SiO_2 (glass phase) on the sintering behavior, TGA, and the THz properties of ZnTiO3 nanopowder were investigated. The $ZnTi(Si_2O_5)_2$ crystalline powders are indicative of more uniform grain size distribution and smaller grain size less than 60 nm. The effects of the silica content on the structural, thermal and THz properties can be accredited to the modification in the bulk porosity. The uniform nano-sized, oriented crystal grain produced lower grain defects and grain boundary distortion, which further contributed to the high-quality factor for excellent structural and terahertz properties.

5. References

1. El Nahrawy AM, Abou Hammad AB, Mansour AM (2021) Preparation and Characterization of Transparent Semiconducting Silica Nanocomposites Doped with P2O5 and Al2O3. Silicon. https://doi.org/10.1007/s12633-021-00962-3
2. El Nahrawy AM, Bakr AM, Hammad ABA, Mansour AM (2021) Nano-architecture of CaO/Ag-chitosan nanocomposite by sol gel process: formation and characterization. Egypt J Chem 64:7393–7406. https://doi.org/10.21608/EJCHEM.2021.80608.3995
3. El Nahrawy AM, Abou Hammad AB, Mansour AM (2021) Structural investigation and optical properties of Fe, Al, Si, and Cu-ZnTiO3nanocrystals. Phys Scr 96:115801. https://doi.org/10.1088/1402-4896/ac119e
4. El Nahrawy AM, Hemdan BA, Abou Hammad AB, et al (2021) Modern Template Design and Biological Evaluation of Cephradine-loaded Magnesium Calcium Silicate Nanocomposites as an Inhibitor for Nosocomial Bacteria in Biomedical Applications. Silicon 13:2979–2991. https://doi.org/10.1007/s12633-020-00642-8
5. El Nahrawy AM, Mansour AM, Bakr AM, Abou Hammad AB (2021) Terahertz and UV–VIS Spectroscopy Evaluation of Copper Doped Zinc Magnesium Titanate Nanoceramics Prepared via Sol-Gel Method. ECS J Solid State Sci Technol 10:063007. https://doi.org/10.1149/2162-8777/ac07f9
6. El Nahrawy AM, Abou Hammad AB, bakr AM, et al (2020) Sol–gel synthesis and physical characterization of high impact polystyrene nanocomposites based on Fe2O3 doped with ZnO. Appl Phys A Mater Sci Process. https://doi.org/10.1007/s00339-020-03822-w
7. Bakr AM, Abou Hammad AB, Wassel AR, et al (2021) Influence of Al, Fe, and Cu on the microstructure, diffused reflectance, THz, and dielectric properties for ZnTiO3 nanocrystalline. Int J Mater Eng Innov 12:115–133. https://doi.org/10.1504/IJMATEI.2021.115604
8. Nanoceramics and novel functionalized silicate-based magnetic nanocomposites as substitutional disinfectants for water and wastewater purification | Enhanced Reader
9. Dontsova TA, Nahirniak S V., Astrelin IM (2019) Metaloxide nanomaterials and nanocomposites of ecological purpose. J. Nanomater. 2019
10. Moharram MAK, Tohami K, El Hotaby WM, Bakr AM (2016) Graphene oxide porous crosslinked cellulose nanocomposite microspheres for lead removal: Kinetic study. React Funct Polym 101:9–19. https://doi.org/10.1016/j.reactfunctpolym.2016.02.001
11. Abou Hammad AB, Bakr AM, Abdel-Aziz MS, El Nahrawy AM (1234) Exploring the ferroelectric effect of nanocrystalline strontium zinc titanate/Cu: Raman and antimicrobial activity. J Mater Sci Mater Electron 31:7850–7861. https://doi.org/10.1007/s10854-020-03323-9
12. Moharram MA, Ereiba KMT, El Hotaby W, Bakr AM (2015) Synthesis and characterization of graphene oxide/crosslinked chitosan nanaocomposite for lead removal form aqueous solution. Res J Pharm Biol Chem Sci 6:1473–1489
13. Özgür Ü, Alivov YI, Liu C, et al (2005) A comprehensive review of ZnO materials and devices. J. Appl. Phys. 98:1–103
14. Zaiour A, Benhaya A, Bentrcia T (2019) Impact of deposition methods and doping on structural, optical and electrical properties of ZnO-Al thin films. Optik (Stuttg) 186:293–299. https://doi.org/10.1016/j.ijleo.2019.04.132
15. El Nahrawy AM, Soliman AA, Sakr EMM, El Attar HA (2018) Sodium-cobalt ferrite nanostructure study: Sol-gel synthesis, characterization, and magnetic properties. J Ovonic Res 14:193–200
16. Haider AJ, Jameel ZN, Al-Hussaini IHM (2019) Review on: Titanium dioxide applications. Energy Procedia 157:17–29. https://doi.org/10.1016/j.egypro.2018.11.159
17. Fernández-García M, Martínez-Arias A, Hanson JC, Rodriguez JA (2004) Nanostructured oxides in chemistry: Characterization and properties. Chem Rev 104:4063–4104. https://doi.org/10.1021/cr030032f
18. Fernández-García M, Wang X, Belver C, et al (2007) Anatase-TiO2 nanomaterials: Morphological/size dependence of the crystallization and phase behavior phenomena. J

Phys Chem C 111:674–682. https://doi.org/10.1021/jp065661i
19. Nahrawy AME, Hammad ABA, Bakr AM, Wassel AR (2019) Adjustment of morphological and dielectric properties of ZnTiO 3 nanocrystalline using Al 2 O 3 nanoparticles. Appl Phys A Mater Sci Process 125:1–8. https://doi.org/10.1007/s00339-018-2350-6
20. El Nahrawy AM, Ali AI, Abou Hammad AB, Mbarek A (2018) Structural and Optical Properties of Wet-chemistry Cu co-doped ZnTiO3 Thin Films Deposited by Spin Coating Method. Egypt J Chem 61:1073–1081. https://doi.org/10.21608/ejchem.2018.4069.1359
21. Hameed TA, Mohamed F, Mansour AM, Battisha IK (2020) Synthesis of Sm 3+ and Gd 3+ Ions Embedded in Nano-Structure Barium Titanate Prepared by Sol-Gel Technique: Terahertz, Dielectric and Up-Conversion Study . ECS J Solid State Sci Technol 9:123005. https://doi.org/10.1149/2162-8777/abc96b
22. Johnsson M, Lemmens P (2007) Crystallography and Chemistry of Perovskites. Handb Magn Adv Magn Mater. https://doi.org/10.1002/9780470022184.hmm411
23. Khan I, Saeed K, Khan I (2019) Nanoparticles: Properties, applications and toxicities. Arab J Chem 12:908–931. https://doi.org/10.1016/j.arabjc.2017.05.011
24. Al-esnawy AA, Ereiba KT, Bakr AM, Abdraboh AS (2021) Characterization and antibacterial activity of Streptomycin Sulfate loaded Bioglass/Chitosan beads for bone tissue engineering. J Mol Struct. https://doi.org/10.1016/j.molstruc.2020.129715
25. Bakr A, Anis B, El hotaby W (2021) Sounchemical synthesis of Graphene/nano hydroxyapatite composites for potential biomedical application. Egypt J Chem 0:0–0. https://doi.org/10.21608/ejchem.2021.91241.4339
26. El hotaby W, Bakr AM, Ibrahim HS, et al (2021) Eco-friendly zeolite/alginate microspheres for Ni ions removal from aqueous solution: Kinetic and isotherm study. J Mol Struct 1241:. https://doi.org/10.1016/j.molstruc.2021.130605
27. Mansour AM, Abou Hammad AB, El Nahrawy AM (2021) Sol–gel synthesis and physical characterization of novel MgCrO4-MgCu2O3 layered films and MgCrO4-MgCu2O3/p-Si based photodiode. Nano-Structures and Nano-Objects 25:100646. https://doi.org/10.1016/j.nanoso.2020.100646
28. Hemdan BA, Nahrawy AM El, Mansour A-FM, Hammad ABA (2019) Green sol–gel synthesis of novel nanoporous copper aluminosilicate for the eradication of pathogenic microbes in drinking water and wastewater treatment. Environ Sci Pollut Res. https://doi.org/10.1007/s11356-019-04431-8
29. Abou Hammad AB, Elzwawy A, Mansour AM, et al (2020) Detection of 3,4-diaminotoluene based on Sr0.3Pb0.7TiO3/CoFe2O4 core/shell nanocomposite: Via an electrochemical approach. New J Chem 44:7941–7953. https://doi.org/10.1039/d0nj01074j
30. El Nahrawy AM, El-Deen HS, Soliman AA, Mosa WMM (2019) Crystallographic and magnetic properties of Al3+co-doped NiZnFe2O4 nano-particles prepared by sol-gel process. Egypt J Chem 62:925–932. https://doi.org/10.21608/EJCHEM.2018.4504.1397
31. El Nahrawy AM, Abou Hammad AB, Mansour AM (2021) Compositional Effects and Optical Properties of P2O5 Doped Magnesium Silicate Mesoporous Thin Films. Arab J Sci Eng 46:5893–5906. https://doi.org/10.1007/S13369-020-05067-4
32. El Nahrawy AM, Mansour AM, Abou Hammad AB (2021) Spectroscopic Study of Eu3+-Doped Magnesium Lanthanum Phosphate (MLPO) Films on SiO2 Substrate. Silicon. https://doi.org/10.1007/s12633-020-00855-x
33. Nahrawy AME, Moez AA, Saad AM (2018) Sol-Gel Preparation and Spectroscopic Properties of Modified Sodium Silicate /Tartrazine Dye Nanocomposite. Silicon 10:2117–2122. https://doi.org/10.1007/s12633-017-9740-9
34. Azab AA, Mansour AM, Turky GM (2020) Structural, Magnetic, and Dielectric properties of Sr4Fe6O13 ferrite prepared of small crystallites. Sci Rep 10:. https://doi.org/10.1038/s41598-020-61460-x
35. El Nahrawy AM, Elzwawy A, Abou Hammad AB, Mansour AM (2020) Influence of NiO on structural, optical, and magnetic properties of

Al2O3–P2O5–Na2O magnetic porous nanocomposites nucleated by SiO2. Solid State Sci 108:106454. https://doi.org/10.1016/j.solidstatesciences.2020.106454

36. El Nahrawy AM, Mansour AM, Abou Hammad AB, Wassel AR (2019) Effect of Cu incorporation on morphology and optical band gap properties of nano-porous lithium magneso-silicate (LMS) thin films. Mater Res Express 6:016404. https://doi.org/10.1088/2053-1591/aae343
37. El Nahrawy AM, Hemdan BA, Mansour & AM, et al Structural and Opto-Magnetic Properties of Nickel Magnesium Copper Zircon Silicate Nano-Composite for Suppress the Spread of Foodborne Pathogenic bacteria. https://doi.org/10.1007/s12633-021-01295-x
38. Dahshan A, Abou Hammad AB, Aly KA, El Nahrawy AM (2020) Eu 2 O 3 role in the optical and photoluminescence properties of 50 SiO 2 − 7 MgO − 20 ZnO − (23 − x) La 2 O 3 − x Eu 2 O 3 nano-crystalline thin films. 126:19. https://doi.org/10.1007/s00339-019-3207-3
39. Wu SP, Luo JH, Cao SX (2010) Microwave dielectric properties of B2O3-doped ZnTiO3 ceramics made with sol-gel technique. J Alloys Compd 502:147–152. https://doi.org/10.1016/j.jallcom.2010.04.131
40. Abou Hammad AB, Darwish AG, El Nahrawy AM (2020) Identification of dielectric and magnetic properties of core shell ZnTiO3/CoFe2O4 nanocomposites. Appl Phys A Mater Sci Process 126:1–12. https://doi.org/10.1007/s00339-020-03679-z
41. Badr Y, Battisha IK, Nahrawy AMS El, Kamal M (2011) Physical Study of Thin Film and Monolithic Nano-Composites [SiO₂: 11P₂O₅: 3 Al₂O₃: (1.2) Er (1.2, 1.8 and 3) Yb] Prepared by Sol Gel Techniq. New J Glas Ceram 01:69–78. https://doi.org/10.4236/njgc.2011.12012
42. El Nahrawy AM, Mansour AM, Abou Hammad AB, et al (1234) Optical, Functional Impact and Antimicrobial of Chitosan/ Phosphosilicate/Al 2 O 3 Nanosheets. J Inorg Organomet Polym Mater 30:3084–3094. https://doi.org/10.1007/s10904-020-01469-x
43. El Nahrawy AM, Hemdan BA, Abou Hammad AB, et al (2020) Microstructure and Antimicrobial Properties of Bioactive Cobalt Co-Doped Copper Aluminosilicate Nanocrystallines. Silicon. https://doi.org/10.1007/s12633-019-00326-y
44. Chang Y-S, Chang Y-H, Chen I-G, et al (2003) The structure and properties of zinc titanate doped with strontium. J Alloys Compd 354:303–309. https://doi.org/10.1016/S0925-8388(02)01362-2
45. Young RA, Wiles DB (1982) Profile shape functions in Rietveld refinements. J Appl Crystallogr 15:430–438. https://doi.org/10.1107/s002188988201231x
46. Belgaroui H, Loukil M, Karray R, et al (2010) The effect of the combined substitution of NH4+ and Cl- on the structure of [Cs0.8(NH4)0.2]2TeBr5.6Cl0.4 powder. J. Alloys Compd. 499:L5–L8
47. Vaezi MR, Kandjani AE, Nikzad L, et al (2007) Synthesis of Zn2TiO4 and ZnTiO3 nanocomposites by the CBD method. Mater Sci Pol 25:1109–1117
48. Chou X, Zhao Z, Zhang W, Zhai J (2010) Microstructures and dielectric properties of Ba0.5Sr0.5TiO3-Zn2TiO4 composite ceramics with low sintering temperature for tunable device applications. Mater Des 31:3703–3707. https://doi.org/10.1016/j.matdes.2010.03.006
49. Manik SK, Pradhan SK (2006) Preparation of nanocrystalline microwave dielectric Zn2TiO4 and ZnTiO3 mixture and X-ray microstructure characterization by Rietveld method. Phys E Low-Dimensional Syst Nanostructures 33:69–76. https://doi.org/10.1016/j.physe.2005.11.019
50. Mahajan J, Jeevanandam P (2019) Synthesis of Zn2TiO4@CdS Core-shell Heteronanostructures by Novel Thermal Decomposition Approach for Photocatalytic Application. ChemistrySelect 4:12580–12591. https://doi.org/10.1002/slct.201903544
51. Mrázek J, Spanhel L, Matějec V, et al (2021) Nanocrystalline Zn2TiO4 films for distributed Bragg’s reflectors operating in near infrared region. Opt Mater (Amst) 112:110805. https://doi.org/10.1016/j.optmat.2021.110805
52. Chen XY, Wang XZ, Liu FJ, et al (2020) Fabrication of porous Zn2TiO4–ZnO

microtubes and analysis of their acetone gas sensing properties. Rare Met 1–8. https://doi.org/10.1007/s12598-020-01518-x

53. Weber-Anneler H, Arndt RW (1985) Thermal methods of analysis/differential scanning calorimetry in theory and application. Thermochim Acta 85:271–274. https://doi.org/10.1016/0040-6031(85)85579-9
54. Gaisford S, Kett V, Haines PJ (Peter J. (2016) Principles of thermal analysis and calorimetry, 2nd ed. Royal Society of Chemistry, Cambridge
55. Wunderlich B (2007) Thermal analysis of macromolecules. J Therm Anal Calorim 89:321–356. https://doi.org/10.1007/s10973-006-8219-5
56. Galwey AK, Brown ME (1999) Thermal decomposition of ionic solids. Elsevier
57. Nafees M, Liaqut W, Ali S, Shafique MA (2013) Synthesis of ZnO/Al:ZnO nanomaterial: structural and band gap variation in ZnO nanomaterial by Al doping. Appl Nanosci 3:49–55. https://doi.org/10.1007/s13204-012-0067-y
58. Mansour AM (2018) Fabrication and Characterization of a Photodiode Based on 5′,5″-dibromo-o-cresolsulfophthalein (BCP). Silicon 11:1989–1996. https://doi.org/10.1007/s12633-018-0016-9
59. El Nahrawy AM, Hammad ABA, Youssef AM, et al (2019) Thermal, dielectric and antimicrobial properties of polystyrene-assisted/ITO:Cu nanocomposites. Appl Phys A Mater Sci Process 125:46. https://doi.org/10.1007/s00339-018-2351-5
60. Mansour AM, Radaf IME, Hameed TA, et al (2019) INVESTIGATION OF Ag2HgI4 NANOPARTICLES: THERMAL PHASE TRANSITION AND NON-ISOTHERMAL KINETIC STUDY. UPB Sci Bull Ser B Chem Mater Sci 81:133
61. Labus N, Mentus S, Rakić S, et al (2015) Reheating of zinc-titanate sintered specimens. Sci Sinter 47:71–81. https://doi.org/10.2298/SOS1501071L
62. P S, V G, K B S (2015) Synthesis Characterization and Photoprotection Properties of ZnTiO3 Powder Prepared by Co-Precipitation Method. Int J Adv Mater Sci Eng 4:33–39. https://doi.org/10.14810/ijamse.2015.4305
63. Bhugul VT, Choudhari GN (2015) Synthesis and Studies on Nanocomposites of polypyrrole-Al- doped zinc oxide Nanoparticles. Int J Sci Res Publ 5:1–5
64. Beigi H, Bindu VH, Hamoon HZR, Rao K V (2011) Low temperature synthesis and characterization of ZnTiO 3 by sol-gel method. J Nano- Electron Phys 3:47–52